A Complete Dual-Cross Pattern for Unconstrained Texture Classification

Swalpa K. Roy, Bhabatosh Chanda,
Bidyut B. Chaudhari
Indian Statistical Institute, Kolkata
swalpa@ieee.org, {chanda,bbc}@isical.ac.in

Dipak K. Ghosh
NIT Rourkela, Orissa
dipak@ieee.org

Shiv Ram Dubey
IIIT Chittoor, Sri City
srdubey@iiits.in

Abstract

*In order to perform unconstrained texture classification this paper presents a novel and computationally efficient texture descriptor called Complete Dual-Cross Pattern (*CDCP*), which is robust to gray-scale changes and surface rotation. To extract* CDCP*, at first a gray scale normalization scheme is used to reduce the illumination effect and, then* CDCP *feature is computed from holistic and component levels. A local region of the texture image is represented by it's center pixel and difference of sign-magnitude transform (*DSMT*) at multiple levels. Using a global threshold, the gray value of center pixel is converted into a binary code named* DCP *center (*DCP_C*).* DSMT *decomposes into two complementary components: the sign and the magnitude. They are encoded respectively into* DCP*-sign (*DCP_S*) and* DCP*-magnitude (*DCP_M*), based on their corresponding threshold values. Finally,* CDCP *is formed by fusing* DCP_S*,* DCP_M *and* DCP_C *features through joint distribution. The invariance characteristics of* CDCP *are attained due to computation of pattern at multiple levels, which makes* CDCP *highly discriminative and achieves state-of-the-art performance for rotation invariant texture classification.*

1. Introduction

Texture classification is one of the active research topics due to scientific challenges and potential use in a wide range of practical applications such as medical image analysis, remote sensing, fabric inspection, segmentation, content-based image retrieval [18], and iris based biometric recognition [19]. In the past satisfactory performance has been obtained by various techniques only in controlled environment. However, classification of unconstrained texture image is a crucial problem due to wide variation of viewpoints, illumination changes and degraded quality of texture image. Therefore, the design of efficient descriptor is a fundamental problem in texture image classification. Basically, texture representation can be categorized in terms of the employed approaches, e.g. geometrical, structural, model-based, statistical, and signal processing. Earlier texture classification methods focus on the statistical analysis of texture images which include the co-occurrence matrix based approach [7] and filtering based techniques [16]. These methods provide good classification performance as long as both training and test sample images have identical orientations. However, arbitrary rotations which could occur in a real-world scene, affect the performance of the methods. Thus, rotation invariance is a crucial issue to be addressed and attention has been focused on the design of geometrically and photometrically invariant local texture representation [24, 15, 21]. At first Kashyap and Khotanzad proposed circular autoregressive dense approach [8] for the rotation invariance texture classification. Earlier, many other models have been explored for rotation invariance classification, including multi-resolution, hidden Markov model, and Gaussian Markov model. Recently Varma and Zisserman proposed VZ-MR8 [20] and VZ-Patch [21] to learn a texton dictionary from a set of training images, which are rotation and scale invariant and then classified the unknown sample images using learned texton distributions. The downside of these methods are feature extraction and matching complexity which is not favourably good.

In order to gain more robustness, feature extraction is often performed over local region of the image. In 1996 a simple and computationally efficient texture representation, called local binary pattern (LBP) was proposed by Ojala *et al.* [14] for gray scale and rotation texture classification. Other variants of LBP such as DLBP [9], LBP variance (LBPV) [6], completed LBP (CLBP) [5], local derivative pattern (LDP) [23], local wavelet pattern LWP [2], local directional derivative pattern (LDDP) [4], local ternary pattern (LTP) [17] etc. were proposed due to numerous application of LBP in the field of computer vision and pattern recognition such as texture segmentation, face recognition, shape localization and object recognition [11]. However, most descriptors are based on the same basic idea of LBP and extracts only circular isotropic micro structure of the texture image at one level, which is not enough to describe the tex-

2327-0985/17 $31.00 © 2017 IEEE
DOI 10.1109/ACPR.2017.160

ture information. To address the problem of LBPs Ding *et. al.* [1] introduced dual-cross pattern (DCP) for face recognition, where DCP feature are computed locally at two levels: *component* and *holistic* levels. Though DCP achieves sufficient robustness under different geometric variations but it loses the information about magnitude of differences and also not carry any information of the referenced pixels.

To address the aforementioned problems this paper proposes a new, simple yet highly discriminative feature descriptor called complete dual-cross pattern (CDCP) to generalize the DCP for rotation invariant texture classification, inspired from CLBP [5]. In CDCP, a local region of the texture image is represented by it's center pixel and difference of sign-magnitude transform (DSMT) at multiple levels. The gray value of center pixel is converted into a binary code named DCP center (DCP_C) using a global threshold. The DSMT decomposes into sign and magnitude components, and they are separately encoded as DCP-sign (DCP_S) and DCP-magnitude (DCP_M) based on their corresponding threshold values. Finally, CDCP is formed by fusing DCP_S, DCP_M and DCP_C components, based on their joint distribution. The CDCP which is computed at multiple levels and inherently includes the informations of center pixel, and complementary sign and magnitude information of DSMT, achieves state-of-the-art performance for rotation invariant texture classification.

The reminder of the paper is organized as follows. Sec. 2 describes details of the DCP. The proposed framework is demonstrated in Sec. 3. Experimental results are presented in Sec. 4. Finally, the conclusion is drawn in Sec. 5.

2. Dual Cross Pattern

The dual-cross pattern (DCP) [1] is a gray-scale representation which characterizes the spatial structure of the local image texture at multiple levels. The DCP value for a given center pixel $P_c^{i,j}$ at (i,j) of the image I of dimension $M_x \times M_y$ is computed by comparing its gray value $I_c^{i,j}$ with those of its N equal-sampled neighbors within radius R_{in} at component level and comparing gray values of N equal-sampled neighbors within radius R_{in} with the gray values of same directional N equal-sampled neighbors within radius R_{ex} at holistic level (Fig. 1). The n^{th} neighbor of $P_c^{i,j}$ within radius R_{in} (i.e. n^{th} element of $P_{R_{in},N}^{i,j}$) is denoted by $P_{R_{in},N,n}^{i,j}$ having gray value $I_{R_{in},N,n}^{i,j}$ and within radius R_{ex} (i.e. n^{th} element of $P_{R_{ex},N}^{i,j}$) is denoted by $P_{R_{ex},N,n}^{i,j}$ having gray value $I_{R_{ex},N,n}^{i,j}$ as shown in Fig. 1, where n is positive integer and $n \in [0, N-1]$. The spatial coordinate (x,y) of $P_{R,N,n}^{i,j}$ within radius R with respect to the origin of the image is given as,

$$\begin{aligned} x(P_{R,N,n}^{i,j}) &= i + r(P_{R,N,n}^{i,j}) \times \cos(\theta(P_{R,N,n}^{i,j})) \\ y(P_{R,N,n}^{i,j}) &= j - r(P_{R,N,n}^{i,j}) \times \sin(\theta(P_{R,N,n}^{i,j})) \end{aligned} \tag{1}$$

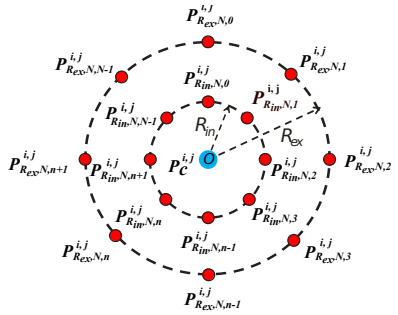

Figure 1: The local neighbors $P_{R_{in},N,n}^{i,j}$ within radius R_{in} and $P_{R_{ex},N,n}^{i,j}$ within radius R_{ex} for $(\forall n \in [0, N-1])$ of a center pixel $P_c^{i,j}$ in polar coordinate system.

where $i \in [R+1, M_x - R]$ and $j \in [R+1, M_y - R]$. $r(P_{R,N,n}^{i,j})$ and $\theta(P_{R,N,n}^{i,j})$ denote the polar coordinates of $P_{R,N,n}^{i,j}$ within radius R and for $n = 0, 1, \ldots, N-1$ values computed as

$$\begin{aligned} r(P_{R,N,n}^{i,j}) &= R \\ \theta(P_{R,N,n}^{i,j}) &= n \times \frac{2\pi}{N} \end{aligned} \tag{2}$$

The DCP encoding of the sample points is realized using two steps. The texture information in each of the N directions is independently encoded and then the pattern in all N directions are combined to form DCP code. To quantize the texture information in each directions DCP is assigned a unique number as follows,

$$\text{DCP}_n = s(I_{R_{in},N,n}^{i,j} - I_c^{i,j}) \times 2 + s(I_{R_{ex},N,n}^{i,j} - I_{R_{in},N,n}^{i,j})$$

Where s is the *unit step* function to find whether a given input is positive or not. The final value of DCP code is computed as

$$\text{DCP}_{(R_{in},R_{ex},N)}^{(i,j)} = \sum_{n=0}^{N-1} \text{DCP}_n \times 4^n. \tag{3}$$

In Fig. 1, we consider equally spaced $N = 8$ sample points of the local neighbors in eight directions of range 0° to 360°, the DCP_n $(i \in [0,7])$ represent discreet variable with four possible decibel values: 0, 1, 2 and 3. Therefore, the total number of distinct levels in DCP code (Eqn. 3) will be $4^8 = 65536$. This value is too large, so for practical implementation, the eight direction are grouped into two cross subsets represented as $\{\text{DCP}_0, \text{DCP}_2, \text{DCP}_4, \text{DCP}_6\}$ and $\{\text{DCP}_1, \text{DCP}_3, \text{DCP}_5, \text{DCP}_7\}$. Each subset is further formulated as an encoder, DCP-1 for first subset and DCP-2 for the next one. In this way, total numbers of levels in dual-cross DCP encoding reduces to $2 \times 4^4 = 512$. The codes produced by DCP-1 and DCP-2 for each reference pixel are

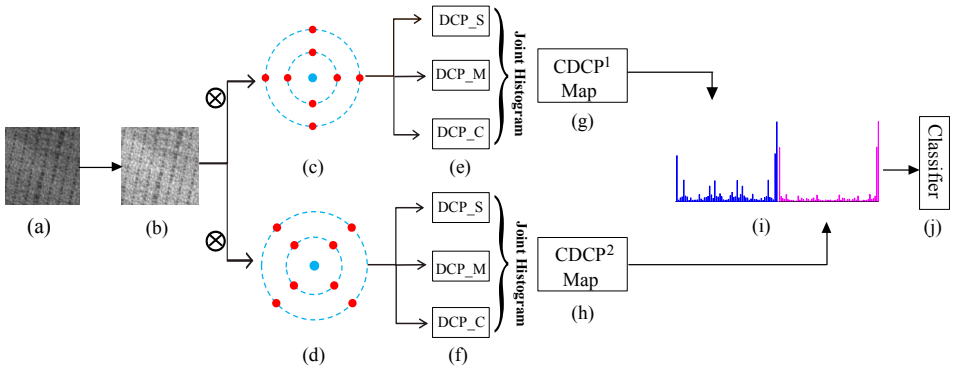

Figure 2: Proposed texture classification framework: (a) Original image. (b) Normalized texture image. (c)-(d) Local sampling structure of DCP-1 and DCP-2. (e)-(f) represent sign, magnitude and center components of DCP-1 and DCP-2. (g)-(h) represent joint histogram map of sign, magnitude and center components for DCP-1 and DCP-2. (i) represents complete dual-cross pattern (CDCP) histogram. (j) Classifier.

represented as,

$$\begin{aligned} \text{DCP} - 1 &= \sum_{n=0}^{3} \text{DCP}_{2n} \times 4^n \\ \text{DCP} - 2 &= \sum_{n=0}^{3} \text{DCP}_{2n+1} \times 4^n. \end{aligned} \tag{4}$$

The final dual-cross DCP descriptor for each referenced pixel of an image is formed by concatenating of two codes generated by DCP-1 and DCP-2 encoders:

$$\text{DCP} = \{\sum_{n=0}^{3} \text{DCP}_{2n} \times 4^n, \sum_{n=0}^{3} \text{DCP}_{2n+1} \times 4^n\} \tag{5}$$

Eqn. (5) shows that DCP is computed very efficiently by only the double time cost of basic LBP.

3. Proposed Framework

This paper proposes a texture classification framework (Fig. 2) which consist of three major step: Image normalization, Complete Dual-Cross Pattern feature extraction, and Classification. In normalization step (Fig. 2(b)), each image sample is preprocessed: normalized to have an average intensity of 128 and a standard deviation of 20 which removes the global intensity and enhanced the contrast.

3.1. Complete Dual-Cross Pattern

Though DCP is a well-known and highly discriminative face descriptor which computes pattern within a local neighborhood at multiple levels and achieves sufficient robustness under different geometric variations, it loses the information about magnitude difference and do not carry the referenced pixel information. To address the aforementioned problems, this paper proposes a new feature descriptor called complete Dual-Cross Pattern (CDCP) to further generalize the DCP descriptor. In CDCP a local region is represented by its referenced pixel and a difference of sign-magnitude transform (DSMT) at *component* and *holistic* level. The details of CDCP descriptor is as follows:

3.1.1 Difference of Sign-Magnitude Transform

Referring the Fig. 1, for a given referenced pixel $P_c^{i,j}$ total difference due to the differences at *component* and *holistic* levels in each of equally spaced N neighboring sample points directions can be represent as

$$\begin{aligned} d_n &= (I^{i,j}_{R_{in},N,n} - I^{i,j}_c) + (I^{i,j}_{R_{ex},N,n} - I^{i,j}_{R_{in},N,n}) \\ &= d^c_n + d^h_n \end{aligned} \tag{6}$$

where $d^c_n = (I^{i,j}_{R_{in},N,n} - I^{i,j}_c)$ and $d^h_n = (I^{i,j}_{R_{ex},N,n} - I^{i,j}_{R_{in},N,n})$ represent *component* and *holistic* level differences, and $n \in [0, N-1]$. The d_n can be further decompose into sign and magnitude components:

$$d_n = s^c_n * m^c_n + s^h_n * m^h_n \tag{7}$$

where $s^c_n = sign(d^c_n)$ and $s^h_n = sign(d^h_n)$ are signs of *component* and *holistic* levels differences, and $m^c_n =\mid d^c_n \mid$ and $m^h_n =\mid d^h_n \mid$ are magnitudes of *component* and *holistic* levels differences. The difference vector and transformed sign and magnitude vectors of *component* and *holistic* levels for equally spaced N neighboring sample points can be represented as $[d_0, d_1, \ldots, d_{N-1}]$, $[s^c_0, s^c_1, \ldots, s^c_{N-1}]$, $[m^c_0, m^c_1, \ldots, m^c_{N-1}]$, $[s^h_0, s^h_1, \ldots, s^h_{N-1}]$, and $[m^h_0, m^h_1, \ldots, m^h_{N-1}]$, respectively. Obviously, vectors $[s^c_0, s^c_1, \ldots, s^c_{N-1}]$ and $[m^c_0, m^c_1, \ldots, m^c_{N-1}]$ are complementary at *components* level, vectors $[s^h_0, s^h_1, \ldots, s^h_{N-1}]$ and $[m^h_0, m^h_1, \ldots, m^h_{N-1}]$ are complementary at *holistic* level, and as per Eqn. (7) the vector $[d_0, d_1, \ldots, d_{N-1}]$

can be perfectly reconstructed using sign and magnitude vectors at *components* and *holistic* levels.

3.1.2 DCP_S, DCP_M, DCP_C, and CDCP

Sec. 3.1.1 describes details of the differences of sign-magnitude components for a referenced pixel at multiple levels. Fig. 2(e) & (f) show three operators namely DCP_C, DCP_S, and DCP_M which are proposed to encode the center gray value (C), sign of difference (S) and magnitude of difference (M) features for DCP-1 and DCP-2, respectively. The DCP_S, DCP_M and DCP_C operators for DCP-1 are defined as

$$\begin{aligned}
\text{DCP_}S^1 &= \sum_{n=0}^{3}(f(d_{2n}^c, 0) \times 2 + f(d_{2n}^h, 0) \times 4^n \\
\text{DCP_}M^1 &= \sum_{n=0}^{3}(f(m_{2n}^c, c_m) \times 2 + f(m_{2n}^h, c_m) \times 4^n \\
\text{DCP_}C^1 &= f({I_c}^{2n}, c_c), \ \ \therefore n = 0, 1, 2, 3 \\
f(x, y) &= \begin{cases} 1, & if\ x \geq y \\ 0, & otherwise. \end{cases}
\end{aligned} \tag{8}$$

where d_{2n}^c and d_{2n}^h represent differences at *component* and *holistic* levels, respectively while m_{2n}^c and m_{2n}^h represent magnitude of d_{2n}^c and d_{2n}^h respectively. c_m is the adaptive threshold value obtained from the mean value of m_{2n} and c_c is threshold value obtained from average gray value of entire image I. Similarly, the DCP_S, DCP_M and DCP_C operators for DCP-2 are defined as

$$\begin{aligned}
\text{DCP_}S^2 &= \sum_{n=0}^{3}(f(d_{2n+1}^c, 0) \times 2 + f(d_{2n+1}^h, 0) \times 4^n \\
\text{DCP_}M^2 &= \sum_{n=0}^{3}(f(m_{2n+1}^c, c_m) \times 2 + f(m_{2n+1}^h, c_m) \times 4^n \\
\text{DCP_}C^2 &= f({I_c}^{2n+1}, c_c), \ \ \therefore n = 0, 1, 2, 3
\end{aligned} \tag{9}$$

here, the adaptive threshold value c_m is calculated from the mean value of m_{2n+1}.

Finally, three defined operators DCP_S^1, DCP_M^1, and DCP_C^1 are combined through joint distribution. Initially, we build a 3-$\mathbb{D}$ joint histogram of DCP_S^1, DCP_M^1, and DCP_C^1, which we referred as CDCP^1 map for DCP-1 shown in Fig. 2(g) and then converted the 3-$\mathbb{D}$ histogram to a 1-$\mathbb{D}$ histogram shown in Fig. 2(i). In a similar way, for DCP-2, DCP_S^2, DCP_M^2, and DCP_C^2 are combined to build CDCP^2 map shown in Fig. 2(h) and 1-$\mathbb{D}$ histogram shown in Fig. 2(i). Finally, the Complete Dual-Cross Pattern (CDCP) histogram is formed by concatenating both 1-$\mathbb{D}$ histograms of CDCP^1 and CDCP^2 maps.

3.2. Similarity Measurement of CDCP histogram

There are several metric for similarity measurement between two histograms such as histogram intersection, log-likelihood ratio and χ^2 metrics. In this work, the texture classification is performed via non-parametric NNC classifier. The NNC with χ^2-distance [15, 21] is used to show the effectiveness of the proposed CDCP descriptor. Two histograms $H_1 = u_1, \ldots, u_M$ and $H_2 = w_1, \ldots, w_M$, are compared using χ^2 distance, defined as $D(H_1, H_2)$ given below.

$$D(H_1, H_2) = \sum_{i=1}^{M} \frac{(u_i - w_i)^2}{u_i + w_i} \tag{10}$$

where M represents the total number of bins, H_1 and H_2 represent the extracted features of a trained model and test sample. The class of test sample H_1 is assigned to the class of trained model H_2 for which the χ^2-distance is minimized.

Table 1: Summary of Texture Database used in Experiment

Texture Database	Image Rotation	Illumination Variation	Scale Variation	Texture Classes	Sample Size (pixels)	Samples per Class	Total Samples
Outex_TC10	✓			24	128 x 128	180	4320
Outex_TC12	✓	✓		24	128 x 128	200	4800

4. Result & Discussion

To figure out the texture classification performance of the proposed Complete Dual-Cross Pattern CDCP descriptor, the experiments are carried out on two large and commonly used well-known Outex_TC_00010 (Outex_TC10) and Outex_TC_00012 (Outex_TC12) [13] texture databases. These databases contain 24 classes of homogeneous texture images each of size 128 $\times$ 128 pixels. **Outex_TC10** contains texture images under illuminant "inca" whereas **Outex_TC12** contains texture images with 3 different lighting conditions ("inca", "horizon", and "t184"). Both of Outex test suit images are collected under 9 different rotation angles ($0^\circ, 5^\circ, 10^\circ, 15^\circ, 60^\circ, 75^\circ$ and 90°) in each texture classes. The test suites **Outex_TC10**, and **Outex_TC12** are summarized in Table 1. Some example images of the Outex database are shown in Fig. 3.

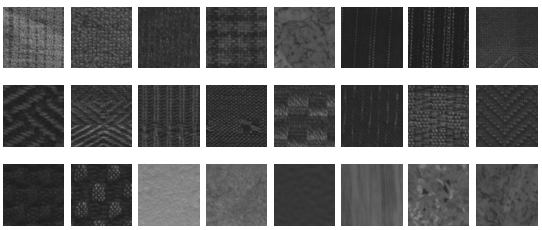

Figure 3: Random samples of 24 texture images having 128 $\times$ 128 pixels each from Outex texture suits

The performance of CDCP descriptor has been evaluated in term of classification accuracy using K-fold cross-

validation test along with non-parametric nearest neighbor classifier (NNC) with Chi-Squre (χ^2) distance. In K-fold cross-validation test, the feature set of each category is randomly sorted and divided into K-folds (K = 10). Average of the classification accuracies over K rounds is computed to get a final cross-validation accuracy. The K-fold cross-validation process provides a more reliable picture of the classification performance. The performance of the proposed descriptor is compared with $\text{LBP}^{riu2}_{R,N}$ [15], DLBP [9], multiscale CLBP_$S/M/C(1,8+3,16+5,24)$ [5], $\text{LDDP}^{riu2}_{R,N}$ [4], LTP [17], PTP [22], BRINT [10], $\text{LBP}^{NT}_{R,N}$ [3], VZ-MR8 [20], VZ-Patch [21], DCP [1] and state-of-the-art methods.

Table 2: Average classification accuracy (%) of CDCP descriptor and state-of-the-art schemes on Outex_TC10 and Outex_TC12

Method	Classifier	Outex_TC10	Outex_TC12		Average
			horizon	t184	
LTP [17]	NNC	76.06	63.42	62.56	67.34
VAR [14]	NNC	90.00	64.35	62.93	72.42
LBP [15]	SVM	97.60	85.30	91.30	88.30
$\text{LBP}^{riu2}_{R,N}$	NNC	84.89	63.75	65.30	64.52
LBP/VAR	NNC	96.56	78.08	79.31	84.65
$\text{LBPV}^{riu2}_{R,N}$ [6]	NNC	91.56	77.01	76.62	76.81
CLBP_S/M/C [5]	NNC	98.93	92.29	90.30	93.05
$\text{LBP}^{NT}_{R,N}$ [3]	NNC	99.24	96.18	94.28	95.23
$\text{DLBP}_{R=3,N=24}$ [9]	SVM	98.10	87.40	91.60	89.50
BRINT [10]	NNC	99.35	97.69	98.56	98.12
VZ-MR8 [20]	NSC	93.59	92.82	92.55	92.99
VZ-Patch [21]	NSC	92.00	92.06	91.41	91.82
PTP [22]	NNC	99.56	98.08	97.94	98.01
LDDP [4]	NNC	97.89	93.40	95.30	94.35
DRLBP [12]	NNC	99.19	95.80	96.72	96.26
DCP [1]	NNC	96.73	97.32	95.83	96.63
Proposed CDCP	NNC	**99.76**	**99.82**	**99.62**	**99.72**

The comparative results of the classification accuracy (%) are tabulated in Table 2. We have made the following observations from the results of the experiment. The classification rate of locally rotation invariant $\text{LBP}^{riu2}_{R,N}/\text{VAR}_{R,N}$ provides better compared to $\text{LBP}^{riu2}_{R,N}$ as $\text{LBP}^{riu2}_{R,N}/\text{VAR}_{R,N}$ computed the joint distribution of LBP and local variance of a texture image which are complementary. CLBP_$S/M/C$(1,8 + 2,16 + 3, 24) which is made by fusing the CLBP_S and CLBP_M/C, provides quite good performance. This is because it contains complementary features of sign and magnitude, in addition to center pixel which represents the gray level of the local patch but multiscale representation of CLBP increases feature extraction and matching complexity which is proportional to its scale. The DLBP + NGF [9], which makes use of the most frequently occurred patterns of LBP to improve the recognition rate is compared with original $\text{LBP}^{u2}_{R,N}$. However, it neglects the local spatial structure which is important for texture discrimination and needs pre training stage for dimensionality selections. The MR8 is a state-of-the-art texton based statistical algorithm, where the VZ-MR8 and VZ-Patch takes dense response from multiple filter. However, the performance is significantly low compared to the proposed CDCP. In addition, feature extraction and matching complexity are quite high [21] because MR8 needs to find 8 maximum responses after 38 filters convolving with the image and compares every 8-dimension vector in an image with all the textons to build histograms using clustering technique. Conventional DCP [1] provides better classification performance compared to LBP, $\text{LBP}^{riu2}_{R,N}$, and $\text{LBP}_{R,N}/\text{VAR}$ because DCP extracts local pattern from *component* and *holistic* levels. But DCP does not incorporate the magnitude information of differences and any information of referenced pixel. In addition, it's performance is significantly less compared to the proposed CDCP. $\text{LBP}^{NT}_{R,N}$ [3] based methods and BRINT [10] give better performance compared to other state-of-the-art LBP methods. However, the accuracies are lower than those obtained by proposed CDCP.

Although the Outex test suits (Outex_TC10 ("inca"), Outex_TC12("horizon" and "t184")) contain both illuminant and different rotation angles, the proposed descriptor achieves performance in term of mean accuracy and standard deviation 99.76 $\pm$ 0.3086%, 99.82 $\pm$ 0.1464, and 99.62 $\pm$ 0.1619 on three different test suits respectively. Table 2 shows proposed CDCP provides better performance compared to state-of-the-art descriptor based texture classification methods because it has the following attributes. It computes local texture pattern from multiple *component* and *holistic* levels which carries more discriminative information of micro as well as macro texture pattern. CDCP is formed by fusing the joint distribution of DCP_S, DCP_M, and DCP_C, therefore it contains complementary components: the sign and magnitude of multi-level differences, as well as gray value of reference pixel. These properties make CDCP descriptor more robust under illumination variation. In addition, the "riu2" mapping scheme is used to individual sign (DCP_S^{riu2}) and magnitude (DCP_M^{riu2}) components for both DCP-1 and DCP-2 (Fig. 2(e)-(f)) to makes CDCP descriptor rotation invariant.

Table 3: The classification accuracy (%) of CDCP descriptor for nine different rotation angles under rotation invariant experimental set-up on Outex test suits.

Databases	Test Angles									Average
	0°	5°	10°	15°	30°	45°	60°	75°	90°	
Outex_TC10	99.79	100	100	99.79	99.58	99.37	99.79	99.58	99.37	99.69
Outex_TC12 (horizon)	100	100	100	99.79	99.79	99.79	99.79	98.33	99.37	99.65
Outex_TC12 (t184)	100	100	100	100	99.37	99.58	99.37	98.95	97.70	99.44

To analyse rotation invariant performance of the proposed descriptor, for both of Outex_TC10 and Outex_TC12, we train the classifier with 8 different rotation angles whereas the classifier was tested using remaining one rotation angle. The classification results of rotation invariant ex-

perimental set-up are tabulated in Table 3. The results show that the proposed descriptor achieves sufficiently high performance in term of mean accuracy and standard deviation $99.69 \pm 0.2354\%$, 99.65 ± 0.5311, and 99.44 ± 0.7511 on Outex_TC10 ("inca"), Outex_TC12 ("horizon" and "t184") test suits respectively.

5. Conclusions

In this paper, we proposed a novel and computationally efficient descriptor named complete dual-cross pattern (CDCP) for illumination and rotation invariant texture image classification by exploring the sign and magnitude components of (DSMT) at *component* and *holistic* levels. In CDCP, three operators DCP_S, DCP_M, and DCP_C were define as the sign and magnitude of multi-level differences and local gray scale features, respectively. Finally, DCP_S, DCP_M, and DCP_C codes, which are in binary string format are combined to build up CDCP by fusing through joint distribution. CDCP is capable to encode micro as well as macro pattern due to extraction of local feature at *component* and *holistic* levels and provides state-of-the-art rotation invariant texture classification performance.

References

[1] C. Ding, J. Choi, D. Tao, and L. S. Davis. Multi-directional multi-level dual-cross patterns for robust face recognition. *IEEE transactions on pattern analysis and machine intelligence*, 38(3):518–531, 2016. 2, 5

[2] S. R. Dubey, S. K. Singh, and R. K. Singh. Local wavelet pattern: A new feature descriptor for image retrieval in medical ct databases. *IEEE Transactions on Image Processing*, 24(12):5892–5903, 2015. 1

[3] A. Fathi and A. R. Naghsh-Nilchi. Noise tolerant local binary pattern operator for efficient texture analysis. *Pattern Recognition Letters*, 33(9):1093–1100, 2012. 5

[4] Z. Guo, Q. Li, J. You, D. Zhang, and W. Liu. Local directional derivative pattern for rotation invariant texture classification. *Neural Computing and Applications*, 21(8):1893–1904, 2012. 1, 5

[5] Z. Guo, L. Zhang, and D. Zhang. A completed modeling of local binary pattern operator for texture classification. *IEEE Transactions on Image Processing*, 19(6):1657–1663, 2010. 1, 2, 5

[6] Z. Guo, L. Zhang, and D. Zhang. Rotation invariant texture classification using lbp variance (lbpv) with global matching. *Pattern recognition*, 43(3):706–719, 2010. 1, 5

[7] R. M. Haralick and K. Shanmugam. Textural features for image classification. *IEEE Transactions on systems, man, and cybernetics*, (6):610–621, 1973. 1

[8] R. L. Kashyap and A. Khotanzad. A model-based method for rotation invariant texture classification. *IEEE Transactions on Pattern Analysis and Machine Intelligence*, (4):472–481, 1986. 1

[9] S. Liao, M. W. Law, and A. C. Chung. Dominant local binary patterns for texture classification. *IEEE transactions on image processing*, 18(5):1107–1118, 2009. 1, 5

[10] L. Liu, Y. Long, P. W. Fieguth, S. Lao, and G. Zhao. Brint: binary rotation invariant and noise tolerant texture classification. *IEEE Transactions on Image Processing*, 23(7):3071–3084, 2014. 5

[11] P. Matti, H. Abdenour, Z. Guoying, et al. Computer vision using local binary patterns, 2011. 1

[12] R. Mehta and K. Egiazarian. Dominant rotated local binary patterns (drlbp) for texture classification. *Pattern Recognition Letters*, 71:16–22, 2016. 5

[13] T. Ojala, T. Maenpaa, M. Pietikainen, J. Viertola, J. Kyllonen, and S. Huovinen. Outex-new framework for empirical evaluation of texture analysis algorithms. In *Pattern Recognition, 2002. Proceedings. 16th International Conference on*, volume 1, pages 701–706. IEEE, 2002. 4

[14] T. Ojala, M. Pietikäinen, and D. Harwood. A comparative study of texture measures with classification based on featured distributions. *Pattern recognition*, 29(1):51–59, 1996. 1, 5

[15] T. Ojala, M. Pietikainen, and T. Maenpaa. Multiresolution gray-scale and rotation invariant texture classification with local binary patterns. *IEEE Transactions on pattern analysis and machine intelligence*, 24(7):971–987, 2002. 1, 4, 5

[16] T. Randen and J. H. Husoy. Filtering for texture classification: A comparative study. *IEEE Transactions on pattern analysis and machine intelligence*, 21(4):291–310, 1999. 1

[17] X. Tan and B. Triggs. Enhanced local texture feature sets for face recognition under difficult lighting conditions. *IEEE transactions on image processing*, 19(6):1635–1650, 2010. 1, 5

[18] M. Tuceryan, A. K. Jain, et al. Texture analysis. *Handbook of pattern recognition and computer vision*, 2:207–248, 1993. 1

[19] S. Umer, B. C. Dhara, and B. Chanda. Iris recognition using multiscale morphologic features. *Pattern Recognition Letters*, 65:67–74, 2015. 1

[20] M. Varma and A. Zisserman. A statistical approach to texture classification from single images. *International Journal of Computer Vision*, 62(1-2):61–81, 2005. 1, 5

[21] M. Varma and A. Zisserman. A statistical approach to material classification using image patch exemplars. *IEEE transactions on pattern analysis and machine intelligence*, 31(11):2032–2047, 2009. 1, 4, 5

[22] K. Wang, C.-E. Bichot, C. Zhu, and B. Li. Pixel to patch sampling structure and local neighboring intensity relationship patterns for texture classification. *IEEE Signal Processing Letters*, 20(9):853–856, 2013. 5

[23] B. Zhang, Y. Gao, S. Zhao, and J. Liu. Local derivative pattern versus local binary pattern: face recognition with high-order local pattern descriptor. *IEEE transactions on image processing*, 19(2):533–544, 2010. 1

[24] J. Zhang, M. Marszałek, S. Lazebnik, and C. Schmid. Local features and kernels for classification of texture and object categories: A comprehensive study. *International journal of computer vision*, 73(2):213–238, 2007. 1